Chinese Journal of Chemical Engineering 67 (2024) 247–256

Contents lists available at ScienceDirect

Chinese Journal of Chemical Engineering

journal homepage: www.elsevier.com/locate/CJChE

Full Length Article

Ethanol steam reforming over Ni/ZSM-5 nanosheet for hydrogen production

Porapak Suriya [1, 2], Shanshan Xu [1, *], Shengzhe Ding [1], Sarayute Chansai [1], Yilai Jiao [3, 4], Joseph Hurd [1], Daniel Lee [1], Yuxin Zhang [1], Christopher Hardacre [1], Prasert Reubroycharoen [5, *], Xiaolei Fan [1, 6, *]

[1] Department of Chemical Engineering, School of Engineering, The University of Manchester, Manchester M13 9PL, United Kingdom
[2] Program of Petrochemistry and Polymer Science, Faculty of Science, Chulalongkorn University, Bangkok, 10330, Thailand
[3] Shenyang National Laboratory for Materials Science, Institute of Metal Research, Chinese Academy of Sciences, Shenyang 110016, China
[4] Liaoning Academy of Materials, Shenyang 110167, China
[5] Center of Excellence in Catalysis for Bioenergy and Renewable Chemicals (CBRC), and, Department of Chemical Technology, Faculty of Science, Chulalongkorn University, Bangkok 10330, Thailand
[6] Nottingham Ningbo China Beacons of Excellence Research and Innovation Institute, University of Nottingham Ningbo China, Ningbo, 315100, China

ARTICLE INFO

Article history:
Received 24 July 2023
Received in revised form
5 December 2023
Accepted 7 December 2023
Available online 8 January 2024

Keywords:
ZSM-5 nanosheet
In situ encapsulation
Ni catalyst
Ethanol steam reforming
Hydrogen production

ABSTRACT

Compared to reforming reactions using hydrocarbons, ethanol steam reforming (ESR) is a sustainable alternative for hydrogen (H_2) production since ethanol can be produced sustainably using biomass. This work explores the catalyst design strategies for preparing the Ni supported on ZSM-5 zeolite catalysts to promote ESR. Specifically, two-dimensional ZSM-5 nanosheet and conventional ZSM-5 crystal were used as the catalyst carriers and two synthesis strategies, *i.e.*, *in situ* encapsulation and wet impregnation method, were employed to prepare the catalysts. Based on the comparative characterization of the catalysts and comparative catalytic assessments, it was found that the combination of the *in situ* encapsulation synthesis and the ZSM-5 nanosheet carrier was the effective strategy to develop catalysts for promoting H_2 production *via* ESR due to the improved mass transfer (through the 2-D structure of ZSM-5 nanosheet) and formation of confined small Ni nanoparticles (resulted *via* the *in situ* encapsulation synthesis). In addition, the resulting ZSM-5 nanosheet supported Ni catalyst also showed high Ni dispersion and high accessibility to Ni sites by the reactants, being able to improve the activity and stability of catalysts and suppress metal sintering and coking during ESR at high reaction temperatures. Thus, the Ni supported on ZSM-5 nanosheet catalyst prepared by encapsulation showed the stable performance with ~88% ethanol conversion and ~65% H_2 yield achieved during a 48-h longevity test at 550 °C.

1. Introduction

Hydrogen (H_2) is a clean energy for the development of a sustainable society and the achievement of Net Zero, yet the current H_2 production routes are not sustainable. For example, almost 50% of H_2 production is based on steam reforming reactions employing natural gas and/or light hydrocarbons [1]. Ethanol is an established renewable platform since its production *via* biomass (such as corn grains and sugarcane) fermentation is the currently major route and economical [2]. Hence, in steam reforming replacement of fossil resources with ethanol, *i.e.*, steam reforming of ethanol (ESR) is one of the promising methods for producing sustainable H_2 [3,4]. The ethanol reforming process involves the following main reactions, *e.g.*, water-gas shift (WGS) and selective oxidation of CO, which is summarized in Eqs. (1)–(3) [5].

$$C_2H_5OH + 3H_2O \rightarrow 2CO_2 + 6H_2 \quad \Delta H = 174\ kJ{\cdot}mol^{-1} \tag{1}$$

$$CO + H_2O \rightarrow CO_2 + H_2 \quad \Delta H = -41\ kJ{\cdot}mol^{-1} \tag{2}$$

$$CO + \frac{1}{2}O_2 \rightarrow CO_2 \quad \Delta H = -283\ kJ{\cdot}mol^{-1} \tag{3}$$

Both noble metals (such as Pt and Rh [6,7]) and transition metals such as (Ni and Co [8,9]) are active for ESR. Comparatively,

* Corresponding authors.
E-mail addresses: shanshan.xu@manchester.ac.uk (S. Xu), prasert.r@chula.ac.th (P. Reubroycharoen), xiaolei.fan@manchester.ac.uk (X. Fan).

https://doi.org/10.1016/j.cjche.2023.12.006

transition metals are desirable due to their low cost and among these Ni-based catalysts are particularly attractive and common reforming catalysts, which are widely used for ESR due to their ability of cleaving C–C, C–H and C–O bond. For example, 10%Ni/$MgAl_2O_4$ catalyst was applied to ESR and exhibited good catalytic performances with 100% of ethanol conversion and 65% of H_2 yield [9]. Although Ni catalysts exhibit good performance in reforming reactions, they are prone to deactivate due to carbon (coke) formation, caused by side reactions such as Boudouard reaction and methane decomposition (Eqs. (4)–(5)) [5].

$$2CO \rightarrow C + CO_2 \quad \Delta H = -172\ \text{kJ·mol}^{-1} \tag{4}$$

$$CH_4 \rightarrow C + 2H_2 \quad \Delta H = 75\ \text{kJ·mol}^{-1} \tag{5}$$

Steam reforming reactions are normally performed at 200–650 °C, and hence, catalyst deactivation at high temperatures is a challenging aspect to be addressed. Regarding the Ni-based reforming catalysts, the preparation of highly dispersed stable supported Ni phases could be achieved by (i) metal phase engineering such as second metal doping to disperse Ni [10] and (ii) metal-support engineering such as confinement synthesis [11]. Regarding the latter, catalyst carriers with the well-defined frameworks and relevant synthesis strategies are needed to confine and stabilize Ni nanoparticles. Zeolites are microporous and crystalline framework materials, which are commonly employed as the catalyst supports for preparing highly dispersed metal catalysts, especially, their well-defined pore networks are beneficial to disperse metal precursors and confine the metal nanoparticles. Recently, a detailed study was performed regarding the siliceous zeolite encapsulated Ni catalysts for dry reforming of methane [12] and the findings suggest that the siliceous zeolite framework encapsulated Ni with small particle sizes showed strong metal-support interactions. Therefore, the catalysts prevented sintering of Ni particles and inhibited coking during dry reforming of methane (DRM) at high temperatures, providing a good catalytic performance. However, in the pristine microporous framework of zeolites, molecular transport can be hindered, which lead to the reduction in the catalyst effectiveness and encourage coking. Therefore, different strategies to improve the species transport within the zeolite-based catalysts are proposed and developed such as hierarchical zeolites and two-dimensional (2-D) zeolites [13,14].

In this work, a 2-D ZSM-5 nanosheet (Z-NS) was prepared and used as the catalyst support to prepare the Ni-based reforming catalysts for ESR due to the reduced diffusion length and high accessibility to active sites in its structure [13,14]. To demonstrate the advantage of Z-NS, conventional ZSM-5 (Z-CON) was synthesized as well for comparison. ZSM-5 was selected as the support because the acidic property can benefit cracking reactions to give small molecules, hence enhancing H_2 production from ESR [15]. To support Ni on the prepared zeolites, two synthesis methods were employed, that is, the direct *in situ* (IN) encapsulation and conventional impregnation. Findings from the characterization of materials and their catalytic performances in ESR suggest that the 2-D structure of Z-NS was beneficial to reduce carbon deposition due to the reduced diffusion resistance. Additionally, the *in situ* encapsulation method contribute to disperse Ni metal precursors and confine the Ni metal nanoparticles within the well-defined lamellar layers of Z-NS, suppressing Ni sintering and carbon deposition significantly, explaining the measured good catalytic performance among the catalysts under investigation.

2. Experimental

2.1. Preparation of catalysts

2.1.1. Chemicals

Tetraethyl orthosilicate (TEOS, ≥99.0%, Sigma-Aldrich) was used as the silica source. Tetrabutylammonium hydroxide (TBAOH: 40% in aqueous solution, Sigma-Aldrich) and tetrapropylammonium hydroxide solution (TPAOH: 40% in aqueous solution, Sigma-Aldrich) were used as the structure directing agents (SDAs). Aluminum isopropoxide (Al(O-i-Pr)$_3$, Sigma-Aldrich) and sodium aluminate ($NaAlO_2$: ≥98.0%, Sigma-Aldrich) were used as the alumina sources. Sodium hydroxide (NaOH: Sigma-Aldrich) and ethylenediamine (EDA: 99%, Fluorochem) were used as a mineralizer and a stabilizing agent, respectively. Nickel nitrate hexahydrate ($Ni(NO_3)_2.6H_2O$: ≥98%, Sigma-Aldrich) was used as the nickel precursor for catalyst preparation. All chemicals were used as received.

2.1.2. Synthesis of ZSM-5 zeolites

ZSM-5 nanosheet (Z-NS) (with the theoretical Si/Al ratio of 100) was synthesized according to the method reported elsewhere [13]. In detail, 8.4 g of TEOS, 8.1 g of TBAOH, and 0.086 g of Al(O-i-Pr)$_3$ were first mixed, then aqueous NaOH solution (0.02 g NaOH in 2.3 ml deionized (DI) water) was added. The precursor mixture was stirred at room temperature for 15 h; Then it was heated at 130 °C for 48 h in an autoclave to prepare the crystalline form. After synthesis, the autoclave was cooled down to room temperature naturally, and the obtained Z-NS was washed using DI water until pH neutral, then separated by centrifugation, and dried at 110 °C overnight. The obtained Z-NS powder was calcined at 550 °C for 5 h with a heating rate of 2 °C·min^{-1}. Note that the mild calcination condition was employed here to maintain the 2-D structure of Z-NS and prevent pore collapsing.

Conventional ZSM-5 (Z-CON) crystal was synthesized by mixing 3.5 g of TEOS, 2.02 g of TPAOH and 0.041 g of $NaAlO_2$, then the addition of aqueous NaOH solution containing 0.07 g of NaOH (in 10.5 ml DI water). The precursor mixture was stirred at room temperature for 2 h and the following synthesis was in the autoclave at 180 °C for 72 h. The obtained Z-CON was washed with DI water until pH neutral, then separated by centrifugation, and dried at 110 °C overnight. The obtained Z-CON powder was calcined at 650 °C for 8 h with a heating rate of 5 °C·min^{-1}.

2.1.3. Preparation of 3%(mass) Ni/ZSM-5 catalysts by impregnation

Zeolites (Z-NS and Z-CON) above in Section 2.1.2 were used as the catalyst supports to prepare the supported Ni catalysts by wet impregnation, which were denoted as Ni/Z-NS-IMP and Ni/Z-CON-IMP, respectively. In detail, 1 g of zeolite was dispersed into the Ni precursor solution containing 0.15 g of $Ni(NO_3)_2{\cdot}6H_2O$ and 5 ml of DI water, the mixture was then stirred at 60 °C for 2 h until it turned to powder. After impregnation, the powder was dried at 110 °C overnight, then the dried Ni/Z-NS-IMP was calcined at 550 °C for 5 h (heating rate of 2 °C·min^{-1}). The dried Ni/Z-CON-IMP catalyst was calcined at 650 °C for 8 h (heating rate of 5 °C·min^{-1}).

2.1.4. Preparation of 3%(mass) Ni/ZSM-5 catalysts by in situ encapsulation

To prepare the zeolite encapsulated Ni catalysts, that is, Ni/Z-NS-IN and Ni/Z-CON-IN, the *in situ* encapsulation method was used [16]. For Ni/Z-NS-IN, same procedure in Section 2.1.2 was used to prepare the Z-NS precursor mixture, *i.e.*, mixing TEOS, Al(O-i-Pr)$_3$, NaOH solution, and TBAOH at the same ratio, Ni precursor solution was prepared by dissolving 0.25 g EDA and 0.38 g $Ni(NO_3)_2{\cdot}6H_2O$ in 1.17 ml DI water, followed by stirring for

2 h (corresponding to the theoretical 3%(mass) Ni loading on 2.52 g zeolite). Then, the Ni precursor solution was added into the Z-NS precursor mixture dropwise followed by stirring for 1 h. Then, the same crystallization and calcination conditions (Section 2.1.2) were used to obtain Ni/Z-NS-IN. Similarly, the same procedures above and that relevant to the synthesis of Z-CON, *i.e.*, mixing of TEOS (3.5 g), $NaAlO_2$ (0.041 g), NaOH solution(0.07 g in 10.5 ml DI water), and TPAOH (2.02 g) at the same ratio, were used to prepare Ni/Z-CON-IN *via* the *in situ* method, in which Ni precursor solution was prepared by dissolving 0.12 g EDA and 0.18 g $Ni(NO_3)_2.6H_2O$ in 0.54 ml DI water (corresponding to the theoretical 3%(mass) Ni loading on 0.18 g zeolite).

2.2. Characterization of materials

The prepared catalysts were characterized comprehensively using powder X-ray diffraction (XRD), X-ray photoelectron spectroscopy (XPS), H_2 temperature-programmed reduction (H_2-TPR), NH_3 temperature-programmed desorption (NH_3-TPD), thermogravimetric analysis (TGA), scanning electron microscopy (SEM), high-resolution transmission electron microscopy (HRTEM), N_2 adsorption–desorption, inductively coupled plasma-optical emission spectrometry (ICP-OES), solid-state nuclear magnetic resonance (NMR) spectroscopy, and energy dispersive X-ray analysis (EDX). Relevant details of the characterization techniques are provided in the Supplementary Material.

2.3. Catalytic ESR

A fixed-bed quartz reactor (O.D. = 6 mm) was used to assess the catalytic performance of the prepared catalysts (pelletized, sizes of 250–425 μm, about 50 mg catalyst for each experiment) in ESR. Before catalysis, the as-prepared catalysts were *in situ* reduced in the reactor by flowing 5%(vol) H_2 (in Ar) at 500 °C for 1 h. During ESR, absolute ethanol at 0 °C and water vapor at 55 °C were introduced to the reactor *via* bubblers with Ar as the carrier gas at flow rates of 65.7 ml·min^{-1} and 27.5 ml·min^{-1}, respectively. The weight hour space velocity (WHSV) was 2286 h^{-1}, calculated by the ratio between the inlet feed (water and ethanol) mass flow rate per hour and the mass of catalyst. The ratio of steam to carbon (S/C) of the reaction system was 11.0. ESR was carried out at 300, 400, 500 and 600 °C to evaluate the activity of the catalysts. All activity data were measured under steady state conditions, *i.e.*, after the introduction of the reactant mixture and stabilization of the feed for 15 min. Each activity measurement was repeated, and the data were averaged (with the standard deviation of ±4.2%). For the longevity test, the ESR was performed at 550 °C for 48 h. All gas products from the reaction systems were analyzed using an online gas chromatograph (GC, PerkinElmer, Clarus® 590), equipped with an HayeSep DB packed column and equipped with a thermal conductivity detector and a flame ionization detector. The kinetic study was conducted using a similar procedure to that described above but with the reduced catalyst loading (about 20 mg, to limit ethanol conversion below 15%) between 200 and 400 °C, and the activation energy (E_a) was calculated using the Arrhenius equation. Ethanol conversion ($X_{Ethanol}$), selectivity to gas products (S_i), and hydrogen yield (Y_{H_2}) are defined by Eqs. (6)–(8).

$$X_{Ethanol} = \frac{F_{in} - F_{out}}{F_{in}} \times 100\% \quad (6)$$

where F_{in} is the inlet molar flow rate of ethanol, and F_{out} is the outlet molar flow rate of ethanol.

$$S_i = \frac{Fc_i}{\sum Fc_{out}} \times 100\% \quad (7)$$

where Fc_i is the molar flow rate of the carbon-containing species i in the gas products, including CO, CO_2, CH_4, CH_3CHO, and C_2H_4 and ΣFc_{out} is the sum of the molar flow rate of C gas products in the gas outlet.

$$Y_{H_2} = \frac{F_{H_2}}{6 \times F_{Ethanol}} \times 100\% \quad (8)$$

where F_{H_2} is the molar flow rate of the produced H_2, and $F_{Ethanol}$ is the molar flow rate of the converted ethanol.

Diffuse reflectance infrared Fourier transform spectroscopy (DRIFTS) of the surface species on the catalysts was performed using a Bruker Tensor 27 FTIR spectrometer during the ESR reaction. Mass flow controllers were used to deliver the gases into the DRIFTS cell during the characterization. Prior to the DRIFTS analysis, the catalysts were reduced at 500 °C for 1 h. After that, the catalysts were quickly transferred to a ceramic crucible cell and were pre-treated at 300 °C for 30 min in a 10%(vol) H_2/Ar flow to remove the re-oxidization by air exposure. Prior to introducing the feed gas, the background spectra were collected at 30 °C under Ar. Then the feed gas mixture (0.2%(vol) ethanol, 1.0%(vol) water with 98.8%(vol) Ar) was fed into the cell under isothermal conditions at 350 °C with a total flow rate of 50 ml·min^{-1}, and the DRIFTS were recorded every 60 s.

3. Results and Discussion

3.1. Physical properties of the materials

The calcined catalysts were characterized by XRD, as shown in Fig. S1 in Supplementary Material The diffraction characteristic peaks of ZSM-5 were observed at 2θ of 8.1°, 9.0°, 14.1°, 15.0°, 23.3°, 24.2°, 24.6° and 45.0° (Fig. S1(b)) and are consistent with the previous findings [17]. After calcination, NiO was observed from characteristic peaks at 2θ of 37.2°, 43.3° and 62.4°, corresponding to the (100), (200) and (220) facets, respectively, [18] as shown in Fig. 1(a).

Fig. 1 and Fig. S2 showed the morphology of the ZSM-5 zeolites and the ZSM-5 supported Ni catalysts (with the Ni particle size distributions in the Fig. 1 insets) from TEM and SEM characterization. Fig. 1(a) and S2(a) shows that Z-NS and supported Ni catalyst had an assembly of thin zeolitic sheets with the average sizes of about 200 nm. The thickness of the lamellar stacks with the MFI framework was 10–20 nm. Conversely, Z-CON particles are coffin-shaped with diameters of 0.5–2.3 μm, as shown in Fig. 1(b). The difference in morphologies of the materials under investigation could be due to different synthesis protocols and types of SDAs. The Z-NS was synthesized using TBAOH with the extended aging time of 15 h to enable the nucleation of the silica-alumina gel. The crystallization of Z-NS was undertaken at 130 °C (for 48 h) to slow down the crystallization rate, and hence allowing the slow rearrangement of aluminosilicate to assemble the 2-D Z-NS with small particle sizes. In contrast, the synthesis of Z-CON employed TPAOH for a shorter aging time (2 h), and the crystallization required an extended synthesis time (72 h) at a higher temperature (180 °C). An increase in synthesis time and/or temperature could induce substantial crystallization and the formation of three-dimensional (3-D) coffin-shaped particles [19] (Figs. S2(c) and S2(d)).

For the zeolite-supported Ni catalysts, the distributions of O, Al, Si, and Ni elements on the prepared catalysts were studied by SEM-

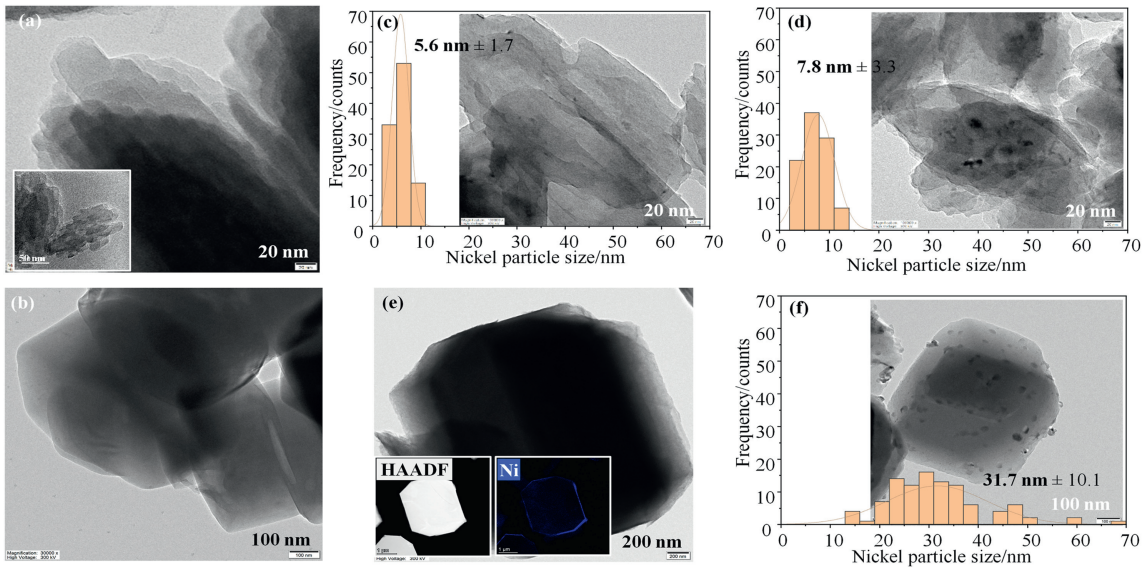

Fig. 1. TEM and high-angle annular dark-field imaging (HAADF) images of the ZSM-5 zeolites and the catalysts based on them (including the Ni particle size distribution): (a) Z-NS, (b) Z-CON, (c) Ni/Z-NS-IN, (d) Ni/Z-NS-IMP, (e) Ni/Z-CON-IN, and (f) Ni/Z-CON-IMP (The particle size distribution were calculated based on 100 Ni particles).

EDS mapping (Fig. S3), showing successful loading of Ni species on all the catalysts. The actual Ni loading of the catalysts was analyzed by ICP-OES, showing that the actual loading amount was 2.6%–3.0%(mass) (Table S1).

Regarding the Ni particle sizes in the catalysts, the following order was found, *i.e.*, Ni/Z-NS-IN (~5.6 nm) < Ni/Z-NS-IMP (~7.8 nm) < Ni/Z-CON-IMP (~31.7 nm). Ni/Z-NS-IN and Ni/Z-NS-IMP showed narrower Ni particle size distribution compared to that of Ni/Z-CON-IMP. Specifically, small Ni nanoparticles in Ni/Z-NS-IN are found to be uniformly distributed within the layers of the laminated 2-D crystal sheets of Ni/Z-NS-IN (Fig. 1(c)), whilst larger Ni particles were identified for Ni/Z-NS-IMP (Fig. 1(d)), and they occupied positions in-between the laminated 2-D crystal sheets of Z-NS. Regarding the Ni/Z-CON-IN catalyst, neither TEM nor high-angle annular dark-field imaging (HAADF) characterization could identify Ni particles on the external surface of zeolite, whilst the corresponding elemental mapping analysis showed the Ni species on the edge of zeolite (Fig. 1(e)), suggesting that most of the Ni nanoparticles might be embedded/encapsulated within the large Z-CON crystals. Comparatively, Ni/Z-CON-IMP showed the large Ni particles dispersed on the external surface of zeolite (Fig. 1(f)).

Fig. S4(a) and Table S1 present the N_2 adsorption-desorption isotherms, pore size distribution (PSD), specific surface areas, and pore volumes of the zeolitic materials under investigation. As shown in Fig. S4(a), the pristine Z-NS support and the associated supported Ni catalysts have the type of IV isotherms with hysteresis loops at high relative pressures, suggesting the presence of micropores and mesopores, being consistent with the findings by Feng *et al.* [20]. Also, it is worth noting that the mesopore volumes of the Ni catalysts based on Z-NS are reduced (0.13 $cm^3 \cdot g^{-1}$for 3% Ni/Z-NS-IN and 0.16 $cm^3 \cdot g^{-1}$ for 3%Ni/Z-NS-IMP, respectively) compared to that of the Z-NS support (0.23 $cm^3 \cdot g^{-1}$), indicating inclusion of Ni nanoparticles between the nanosheets of Z-NS occupied the mesopore value. Comparatively, Z-CON and 3%Ni/Z-CON-IMP show similar N_2 adsorption-desorption isotherms with comparable surface area (of ~338 $m^2 \cdot g^{-1}$) and pore volume (of ~0.20 $cm^3 \cdot g^{-1}$) only with the presence of micropores, whilst 3% Ni/Z-CON-IN shows a small hysteresis loop at high pressure with higher surface area of 376 $m^2 \cdot g^{-1}$, suggesting the formation of mesoporous structure/defects during the *in situ* encapsulation synthesis for Ni incorporation [16]. This is evidenced by the pore size distribution as well (Fig. S4(b)). Additionally, 3%Ni/Z-CON-IMP shows a higher external surface area than the pristine Z-CON support (*i.e.*, 70 *vs.* 51 $m^2 \cdot g^{-1}$), indicating the presence of Ni species on the external surface, as suggested by TEM above. As shown in Table S1, the Z-CON support shows a higher microporous volume (V_{micro}) than that of Z-NS (0.15 *vs.* 0.13 $cm^3 \cdot g^{-1}$), suggesting the high crystallinity of Z-CON due to higher hydrothermal temperature and longer aging time during the synthesis (180 °C for 72 h *vs.* 130 °C for 48 h).

3.2. Chemical properties of the materials

Fig. 2 presents the XPS characterization of the calcined catalysts under investigation. For Ni/Z-NS-IMP catalyst, the binding energies (B.E.) of Ni species located at 853.2 (Ni $2p_{3/2}$) and 870.6 (Ni $2p_{1/2}$), respectively, corresponding to the NiO phases, whilst the B.E. at 858.8, and 876.3 eV are satellite peaks of NiO. Regarding Ni/Z-CON-IMP, the Ni $2p_{3/2}$ showed peaks with a B.E. at 853.8 eV for Ni^{2+} (NiO) and at 855.7 eV for Ni^{2+} ($Ni(OH)_2$) suggesting that the support structure affected the chemical state of the impregnated Ni particles and possible interaction between the support Ni with the zeolite framework during the calcination. For the two —IN catalysts, only peaks for Ni^{2+} $2p_{3/2}$ was detected at the B.E. of 855.1 eV (for Ni/Z-NS-IN) and 856.6 eV (for Ni/Z-CON-IN), which is different from the typical B.E. for $Ni(OH)_2$ (*i.e.*, 855.6–855.8 eV). Accordingly, these species could be attributed to the formation of —O-Ni-O— linkages in the zeolite framework since Ni was incorporated into the ZSM-5 framework *via* the *in situ* encapsulation method [21,22].

H_2-TPR spectra of the Ni catalysts are shown in Fig. 3(a). Ni/Z-CON-IN only showed the major reduction peak at the high temperature range of 650–850 °C (corresponding to γ-NiO [23]), confirming the strong interaction between the encapsulated Ni particles and the Z-CON framework, being in line with the XPS results discussed above. In contrast, Ni/Z-CON-IMP showed the main reduction peak at low temperatures centered at about 366 °C (*i.e.*, α-NiO), suggesting NiO weakly deposited on the external surface of Z-CON crystals. Conversely, Ni/Z-NS-IN and Ni/Z-NS-IMP exhibited H_2-reduction behavior consistent with α-NiO (300–500 °C) and β-NiO (500–650 °C, corresponding to bulk NiO species) and γ-NiO

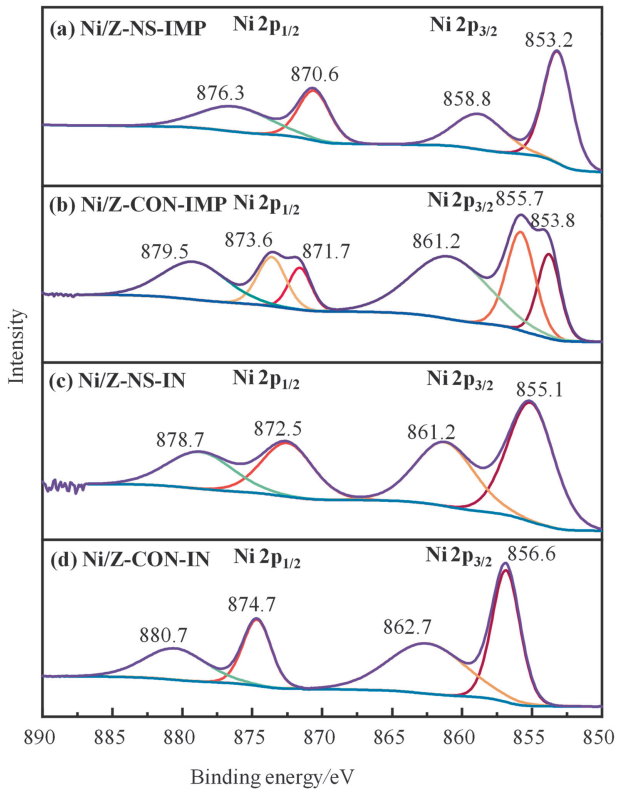

Fig. 2. XPS spectra of the calcined catalyst (a) Ni/Z-NS-IMP, (b) Ni/Z-CON-IMP, (c) Ni/Z-NS-IN, and (d) Ni/Z-CON-IN.

(650–850 °C), suggesting that the 2-D nanosheet structure of Z-NS strengthens the Ni-zeolite interactions. Table S2 shows that the total amount of H_2 consumption of Ni/Z-NS-IN (0.260 mmol·g^{-1}) and Ni/Z-NS-IMP (0.218 mmol·g^{-1}) are higher than that of Ni/Z-CON-IN (0.199 mmol·g^{-1}) and Ni/Z-CON-IMP (0.134 mmol·g^{-1}), suggesting that the nanosheet structure benefited the accessibility of the supported Ni species to H_2 molecules, and this improved accessibility could promote the reduction of the supported Ni species on the carrier. It is worth noting that the -IMP catalysts showed lower amounts of H_2 consumption than the -IN catalysts, which is due to the aggregated large Ni particles prepared by impregnation in comparison with the encapsulated small Ni nanoparticles, in line with the above TEM results.

NH_3-TPD profiles of the zeolites and catalysts are shown in Fig. 3(b), and all showed the NH_3 desorption peaks in a temperature range of 80–350 °C. The calculated total acidity of Z-NS, Ni/Z-NS-IN, and Ni/Z-NS-IMP was about 0.275 mmol·g^{-1}, 0.153 mmol·g^{-1}, and 0.163 mmol·g^{-1}, respectively, as shown in Table S2. In comparison with the bare Z-NS, the Z-NS-supported Ni catalyst showed lower NH_3 desorption temperature and weak acidity (*i.e.*, Lewis acid sites), which was probably due to the interaction between Ni species and the silanol groups of the zeolite support [24]. Similarly, the measured total acidity of Z-CON, Ni/Z-CON-IN, and Ni/Z-CON-IMP were 0.254 mmol·g^{-1}, 0.146 mmol·g^{-1}, and 0.116 mmol·g^{-1}, respectively, and Ni loading caused the decrease in NH_3 desorption temperature and total acidity. Additionally, ^{27}Al solid-state NMR spectra of Z-CON, Z-NS and 3%Ni/Z-NS-IN were recorded to probe the local Al environment in the zeolites under investigation (Fig. S5). A relatively symmetric peak at $\delta\{^{27}Al\}$ ~55 $\times 10^{-6}$, which can be assigned to tetrahedral aluminum in the zeolitic framework [25–27], was observed for all three samples. No evidence of extra-framework Al species was observed. After Ni encapsulation within Z-NS using the *in situ* method, no significant changes were found for the chemical shift and shape of this peak, suggesting that Ni inclusion did not interfere with the tetrahedral coordination in the framework. Findings above show that the catalysts under investigation have similar physicochemical properties, and thus comparative assessment of their activities in ESR can be fair.

3.3. Catalytic ESR over different catalysts

The four Ni catalysts, that is, Ni/Z-NS-IN, Ni/Z-NS-IMP, Ni/Z-CON-IN, and Ni/Z-CON-IMP, were reduced at 500 °C before catalytic ESR. Note that the preliminary study showed that the catalyst reduced at 500 °C (Fig. S6) showed the comparatively best catalytic performance. The reduced catalysts were tested at 300–600 °C, and the activity was presented in the form of ethanol conversion, H_2 yield, and gas product distribution, as shown in Fig. 4. For the -IN catalysts here, reaction rates over them increased gradually by increasing the reaction temperature, as evidenced by the improved ethanol conversions and H_2 yields (Figs. 4(a) and (b), the two -IN catalysts achieved nearly complete ethanol conversions at 600 °C). In detail, over Ni/Z-NS-IN, $X_{Ethanol}$ was enhanced from 1.3% (at 300 °C) to 99.9% (at 600 °C) with Y_{H_2} increased from 11.6% (at 300 °C) to 61.7% (at 600 °C). Comparatively, the $X_{Ethanol}$ and Y_{H_2} over Ni/Z-CON-IN were increased from 1.1% to 99.9% and 0.53%–60.5%, respectively, by increasing reaction temperature from 300 °C to 600 °C.

In addition to H_2, acetaldehyde (CH_3CHO) was identified as the major by-product at 300 °C over the two -IN catalysts (*i.e.*, selectivity to CH_3CHO: 94.2% over Ni/Z-NS-IN and 88.3% over Ni/Z-CON-IN at 300 °C, Figs. S7(a) and (b). CH_3CHO is the product from ethanol dehydrogenation, obtained at low temperatures of 300–400 °C [28], and it can further react with steam (H_2O) to be converted to CO, CO_2

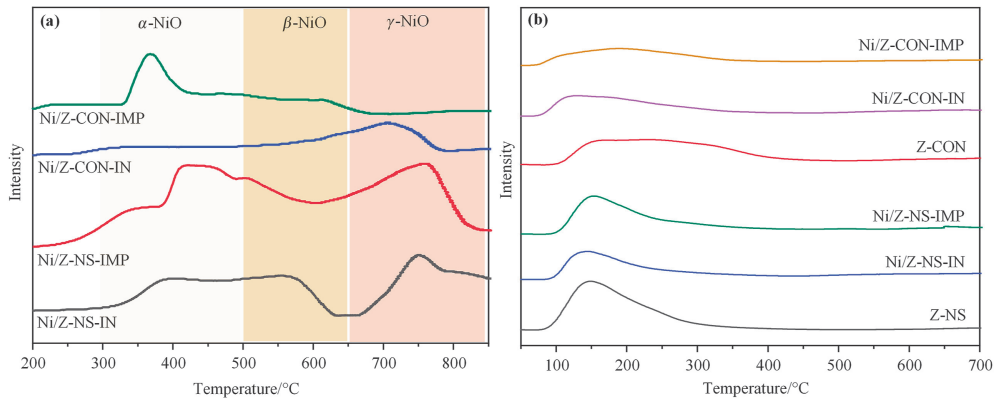

Fig. 3. (a) H_2-TPR and (b) NH_3-TPD profiles of the Ni/ZSM-5 catalysts under investigation.

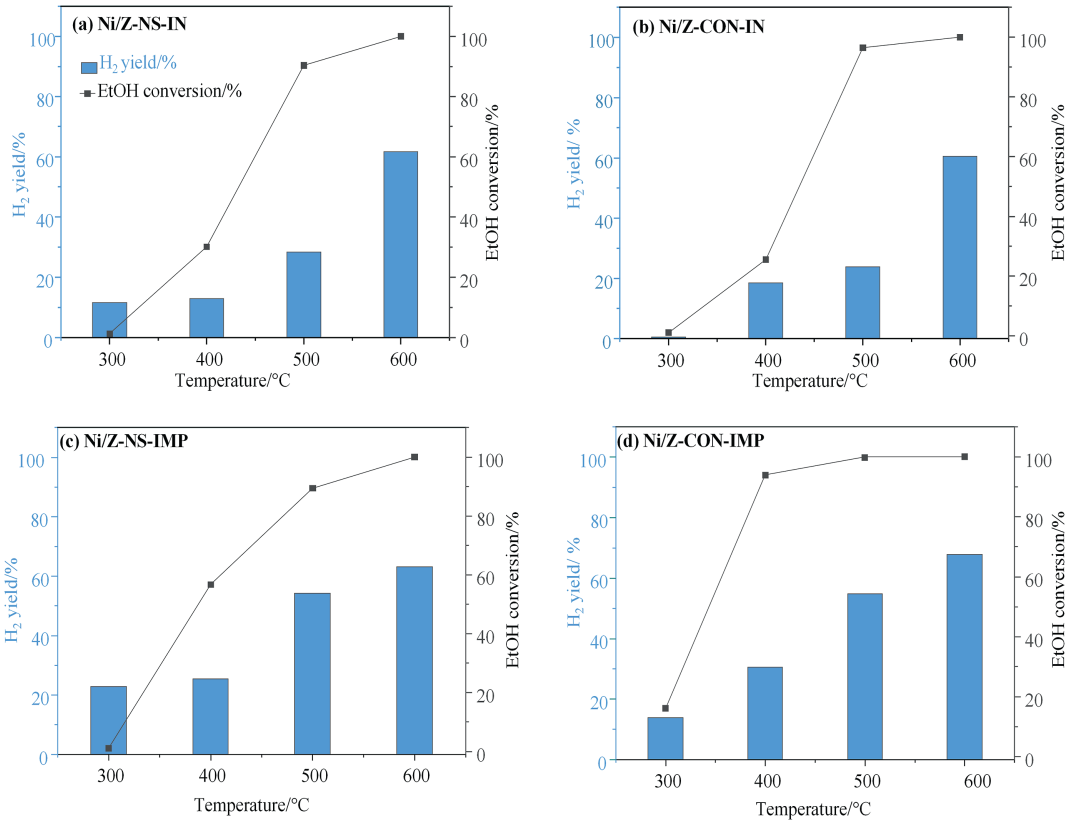

Fig. 4. Effect of temperature on the catalytic performance of -IN and -IMP catalysts in ESR at 300–600 °C: (a) Ni/Z-NS-IN, (b) Ni/Z-CON-IN, (c) Ni/Z-NS-IMP, and (d) Ni/Z-CON-IMP.

and light hydrocarbons of CH_4 and C_2H_4 at elevated temperatures. In our systems, over the two -IN catalysts, increasing temperature to 500 °C reduced the selectivity to CH_3CHO (*e.g.*, to 45.7% for Ni/Z-NS-IN and 75.8% for Ni/Z-CON-IN at 400 °C), whilst the total selectivity to CO, CO_2 and hydrocarbons gently raised (Figs. S7(a) and (b)). Comparative DRIFTS characterization of the two -IN catalysts was conducted at 350 °C, and the similar surface species and intermediates during the ethanol conversion were obtained (Fig. S8), which indicates that the reaction pathways over the two –IN catalysts are similar. C–C bond cleavage on Ni sites in the catalysts occurred with an increase in the reaction temperature [28], and at 600 °C, only CO, CH_4, CO_2 and H_2 were detected in the two systems over the –IN catalysts (Figs. S7(a) and (b)).

Over the two -IMP catalysts, the reaction rates were higher than that over the -IN counterparts, as shown in Fig. 4(c) and (d), especially Ni/Z-CON-IMP which achieved rather high ethanol conversion of ~93.9% and H_2 yield of 30.5% at only 400 °C (Fig. 4d). According to TEM characterization above (Fig. 1), Ni nanoparticles on the catalysts prepared by impregnation were deposited on the external surface regardless of the zeolite morphology. Hence, the good accessibility of Ni nanoparticles to the reactant molecules could contribute to the high ethanol conversions compared with the -IN catalyst (where the Ni particles are confined within the zeolite structure). Regarding the production distribution (apart from H_2) in the two systems using the -IMP catalysts (Figs. S7(c) and (d)), the selectivity of CH_3CHO was prone to be completely converted to light hydrocarbon products at ≤500 °C. At 600 °C, the ESR performance (regarding $X_{Ethanol}$ and Y_{H_2}) of all catalysts were comparable at about 99.9% and 65.0%.

The ESR stability tests of all the catalysts were performed at 550 °C for 48 h, as shown in Fig. 5. Regarding $X_{Ethanol}$ (Fig. 5(a)), the -IN catalysts showed better stability than the -IMP catalysts. In detail, Ni/Z-CON-IN presented a stable performance with almost 100% ethanol conversions until 42 h, followed by a slight deactivation to ~97.6% at 48 h. For Ni/Z-NS-IN catalyst, $X_{Ethanol}$ was stable with 97.7% in the first 6 h and then showed a gradual decrease to ~88.4% at 48 h. Similarly, Ni/Z-NS-IMP catalyst showed stable ethanol conversion of 100% within the first 6 h and then deactivated significantly to ~69.0% over the 48-h experiment. The system employing Ni/Z-CON-IMP showed the significant deactivation, in which $X_{Ethanol}$ decreased considerably from 100% to ~50.2% during the stability test. Based on the measured ethanol conversions from the longevity tests, the -IN catalysts are clearly more stable than the -IMP ones, which could be ascribed to the confinement effect of zeolite to prevent the Ni sintering at high reaction temperature [12]. However, regarding Y_{H_2} (Fig. 5(b)), the NS-supported Ni catalysts showed higher H_2 yields than that of the Z-CON supported catalysts regardless of the preparation methods. Specifically, Ni/Z-NS-IN demonstrated a very stable performance with Y_{H_2} of ~65% over the course of the stability test, while Ni/Z-CON-IMP showed a decreased of Y_{H_2} from 66.0% to 47.8% through the 48-h ESR test, which is caused by the decreased ethanol conversion. It is worth noting that even though the Ni/Z-CON-IN catalyst showed stable and high ethanol conversions (close to 100%), the H_2 yield in the system was comparatively low which was maintained at about 50%, suggesting that significant proportion ethanol was converted to byproducts (such as CH_3CHO and CH_4, as shown in Fig. 5(e)). Hence, the findings suggest that the combination of the encapsulation strategy and the NS carrier was effective to promote H_2 production *via* ESR.

In addition to H_2, other gas products including CO, CO_2, CH_4, C_2H_4, and CH_3CHO were detected during the stability tests at 550 °C, showing that CO_2 and CO as the main products (through main ESR reaction, ethanol and acetaldehyde decomposition,

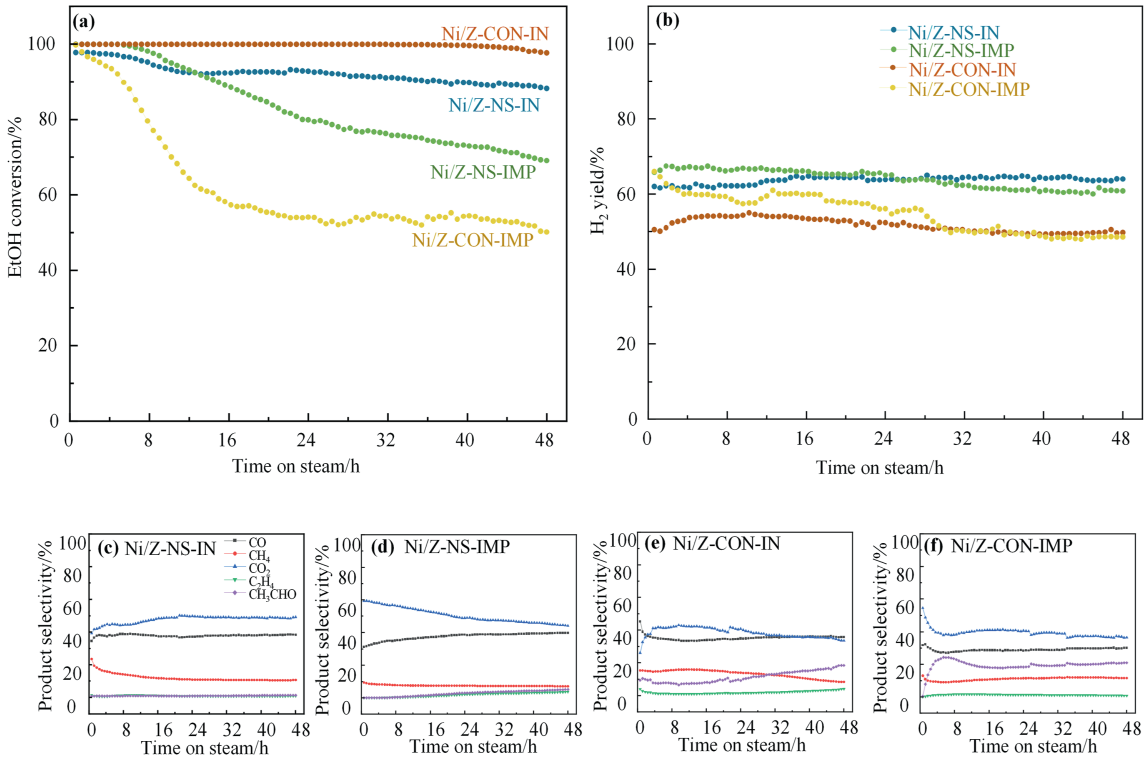

Fig. 5. ESR stability test of the -IN and -IMP catalysts at 550 °C (S/C = 11.0): (a) $X_{Ethanol}$, (b) Y_{H_2}, (b) H_2 yield; And selectivity to gas products over different catalysts: (c) Ni/Z-NS-IN, (d) Ni/Z-NS-IMP, (e) Ni/Z-CON-IN, and (f) Ni/Z-CON-IMP.

water–gas shift reaction, methane steam reforming reactions [29]) from all the systems under investigation. C_2H_4 (from ethanol dehydration), which could contribute to coke formation in the ESR [30], was detected insignificantly due to the low acidity of the ZSM-5 supports (Si/Al = 100), being in line with previous findings over a Ni/SiO_2 catalyst [29]. CH_3CHO (produced *via* dehydrogenation of adsorbed ethanol [29]) is regarded as the key intermediate to form CH_4 and CO in ESR, especially at low temperatures of <450 °C [31–33]. For Ni catalysts supported on Z-CON, ~12% and ~20% of CH_3CHO were observed over the Ni/Z-CON-IN and Ni/Z-CON-IMP catalyst, respectively. Conversely, CH_3CHO was negligible in the systems over the Ni/Z-NS-IN and Ni/Z-NS-IMP catalyst, reflecting the effect of the carrier structure on ESR. In detail, TEM analysis has shown that (i) the Z-CON supports (Fig. 1(b)) are three-dimensional micron-scale crystals and (ii) almost all the Ni species were mainly supported on the outskirt and/or external surface (Fig. 1(e) and (f)) for Ni/Z-CON-IMP catalyst and part of Ni species in Ni/Z-CON-IN was distributed on the edge of zeolite. Therefore, over the Ni catalysts based on the Z-CON support, ethanol molecules could be adsorbed rather easily to allow dehydrogenation in such area, and the formed CH_3CHO could desorb from the Ni surface readily after the reaction and diffuse back to the bulk steam, explaining the comparative significant presence of CH_3CHO in the two systems using Ni/Z-CON-IN and Ni/Z-CON-IMP. In contrast, the catalysts based on Z-NS have small Ni nanoparticles (Fig. 1(c) and (d)) within large mesopore volumes in the NS support (>0.4 $cm^3 \cdot g^{-1}$, Table S1). The accessible 2-D layered structure of the Z-NS catalysts could allow diffusion of the intermediate CH_3CHO within the lamellae to be further decomposed on Ni active sites to give CO and CH_4 ($CH_3CHO \rightarrow CO + CH_4$), suppressing the diffusion of CH_3CHO back to the bulk reaction stream. The presence of CH_4 in the gas streams suggests the direct ethanol decomposition reaction ($CH_3CH_2OH \rightarrow CO + CH_4 + H_2$) and CH_3CHO decomposition reaction in the systems. Therefore, this enhanced mass transfer of intermediate through the 2-D structure of NS and the confined small Ni nanoparticles (prepared *via* the *in situ* encapsulation synthesis) contribute to the promoted H_2 production and high stability of Ni/Z-NS-IN catalysts in ESR.

The crystallinity of the used Ni/Z-NS-IN and Ni/Z-CON-IN catalyst reduced to 90.9% (from 97.2%) and to 92.6% (from 95.8%), respectively, (Fig. S11) compared to the calcined samples, suggesting the insignificant structure changes during the 40-h stability test. The TEM micrographs of the used catalysts after the stability tests are shown in Fig. 6. For the morphology of 3Ni/Z-NS-IN and 3Ni/Z-CON-IN, significant changes were found between the used catalysts and the fresh ones (calcined), as shown in Figs. 1 and 6. Compared to the Z-CON support, Z-NS could suppress Ni sintering to some extents regardless the catalyst preparation methods. Our previous study [12] has shown the effectiveness of the encapsulation method for inhibiting Ni sintering in dry reforming of methane. Here the Ni/Z-NS-IN catalyst exhibited least significant Ni sintering after the 48-h of longevity test, *i.e.*, from about 5.6 nm (Fig. 1(c)) to about 8.7 nm (Fig. 6(a)). For the Ni/Z-NS-IMP catalyst, Ni sintering after the reaction was found more considerably from 7.8 nm (Fig. 1(d)) to about 13.3 nm (Fig. 6(b)). The Z-CON support showed rather poor ability to suppress Ni sintering, and the used Ni/Z-CON-IN catalyst showed large Ni particles (about 31.7 nm, Fig. 6(c)) distributed in the support after the stability test, whilst TEM analysis was not able to show the Ni nanoparticles in the fresh Ni/Z-CON-IN catalyst (Fig. 1(e)). The Ni/Z-CON-IMP catalyst showed the most significant Ni sintering with very large Ni particles (~43.6 nm) identified on the used Ni/Z-CON-IMP catalyst. Overall, although Ni sintering (of the catalysts under investigation) seems inevitable during the 48-h stability tests at high temperature, the combination of *in situ* encapsulation synthesis with the Z-NS support could contribute to suppress this process to obtain the high activity of catalysts for ESR reaction.

Coke formation was found on all the catalysts (as evidenced by TEM) which was reported to form *via* (i) methane decomposition,

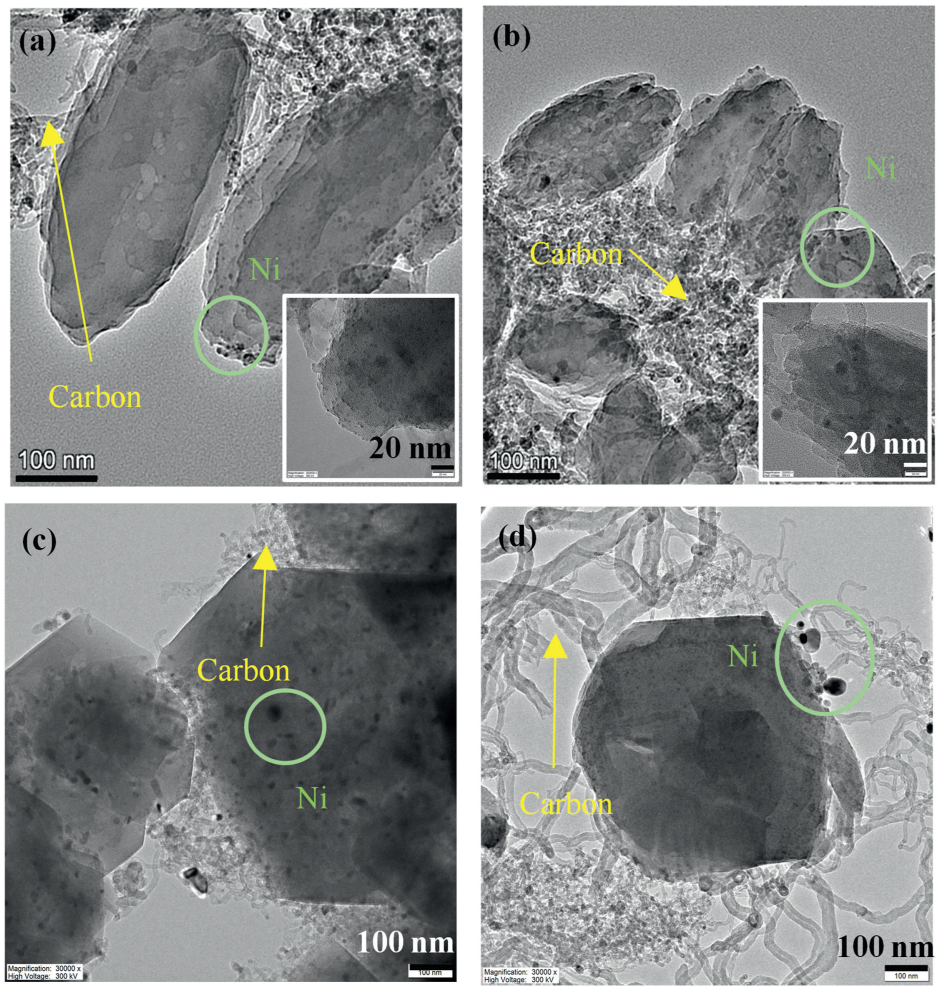

Fig. 6. TEM micrographs of the used catalysts after the stability tests at 550 °C: (a) Ni/Z-NS-IN, (b) Ni/Z-NS-IMP, (c) Ni/Z-CON-IN, and (d) Ni/Z-CON-IMP.

(ii) Boudouard reaction and (iii) ethylene polymerization [29,34]. The filamentous carbon or carbon nanotubes (CNTs) as the main coke type were observed by TEM, which is crystalline (as evidenced by the XRD analysis, Fig. S10), suggesting catalytic methane decomposition as the main mechanism for coking in the systems under investigation [35]. This is reasonable since Ni catalysts are used for catalyzing methane decomposition as well, especially large Ni particles (>7 nm) [36]. This is evidenced by the significant presence of CNTs on the used Ni/Z-CON-IMP catalyst with the comparatively largest Ni particles supported on its outer surface (Fig. 6(d)), which contributed to the severe deactivation of Ni/Z-CON-IMP (Fig. 5(a)).

To further assess carbon deposition on the used catalyst, TGA of the used catalysts was performed, as shown in Fig. 7. The TGA profiles of the used catalysts showed significant mass loss at 430–590 °C, corresponding to the decomposition temperature of CNTs [37], being consistent with the discussion above on carbon deposition based on TEM characterization. The *in situ* encapsulation synthesis method showed the effectiveness for reducing coke deposition on the resulting catalysts due to the confinement effect on the Ni particle growth. For example, the used Ni/Z-NS-IN and Ni/Z-CON-IN catalysts showed the mass loss of ~16% and ~23 %, respectively, whilst the two catalysts prepared by the conventional impregnation method presented similar mass losses of about 32%. Additionally, 2-D structure of the Z-NS support might (i) reduce diffusion resistance of reactive species (such as CH_3CHO and methane as the precursors of coke) during ESR to alleviate coking on the catalyst and/or (ii) suppress the growth of CNTs by trapping them within its lamella structure (as shown in Fig. 6(a) and (b)). Therefore, confinement effect on the small Ni particles and the

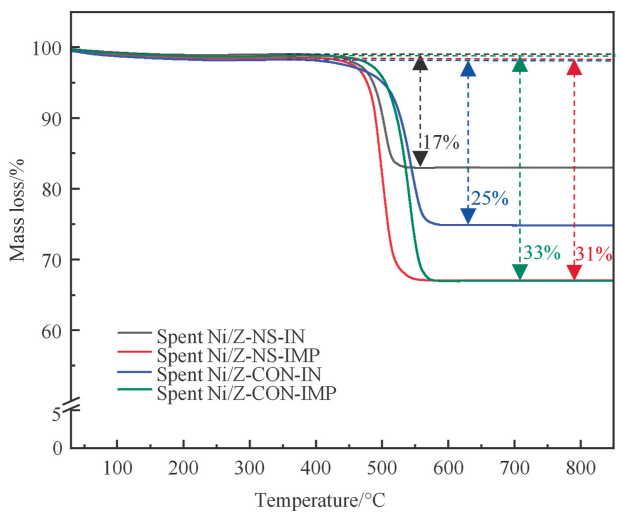

Fig. 7. TGA profiles of the used catalysts after the 48-h ESR stability tests at 550 °C.

reduced diffusion resistance (*i.e.*, enhanced mass transfer) in 2-D nanosheet lead to the suppressed coking over Ni/Z-NS-IN. It is worth noting that Ni/Z-CON-IMP showed the most significant deactivation during the ESR stability test (Fig. 5(a)), suggesting that over Ni/Z-CON-IMP, metal sintering and coking were responsible for the activity loss during ESR.

Based on the results discussed above (Figs. 4 and 5), the -IN catalysts showed better ESR catalytic performances regarding stability than the -IMP catalysts, and Ni/Z-NS-IN presented the best catalytic performance with 65.0% H_2 yield and 88.4% ethanol conversion in a 48-h longevity test. Compared to the relevant state-of-the-arts under similar conditions (Table S3), the Ni/Z-NS-IN catalyst can be ranked top. For example, at comparable weight hourly space velocities (WHSV), the Ni supported on Al_2O_3 catalyst (prepared by a one-pot synthesis method) showed 96% ethanol conversion and 82% H_2 yield at 500 °C (at 2773 h^{-1}), but with significant coke deposition (about 48%(mass) after the 4-h ESR test) [38], which could affect the longevity of the catalyst significantly. Wang *et al.* [39] prepared the Ni on silica catalyst using the *in situ* hydrothermal synthesis method, and the catalyst gave 85% ethanol conversion and 70% H_2 yield at 400 °C through a 100-h ESR test. However, Ni loading on the catalyst was significantly higher (up to 22%(mass)) than Ni/Z-NS-IN (with the Ni loading of only ~3 %(mass)). Kumar *et al.* [40] prepared 10 %(mass) Ni on ZSM-5 (by wet impregnation) for ESR at 600 °C, in which ethanol conversion of 98.5% and H_2 selectivity of 72% were achieved. However, significant coking of the catalyst was measured (*i.e.*, about 25 %(mass) after a 6-h of ESR, whereas it is 16 %(mass) on Ni/Z-NS-IN after 48-h). Other relevant catalytic systems employing catalysts based on conventional zeolite supports also experienced rather significant coking after first few hours [10,41,42]. Hence, the combination of the *in situ* (encapsulation) hydrothermal method and the 2-D Z-NS structure is the key for the stable performance of the Ni/Z-NS-IN catalyst in ESR with the contribution from the stabilized small Ni particles and reduced diffusion lengths.

Kinetic studies (at low ethanol conversions of <15%) were conducted to further evaluate the activity of the catalysts by calculating the overall activation energy (E_a, using Arrhenius equation) of ESR. Fig. 8 shows the Arrhenius plots of the four catalysts under investigation. The calculated E_a values of the -IN catalysts are 66 and 88 kJ·mol^{-1}, respectively, for Ni/Z-NS-IN and Ni/Z-CON-IN, being lower than that of the -IMP catalysts (*i.e.*, 105 kJ·mol^{-1} for Ni/Z-NS-IMP and Ni/Z-CON-IMP for 93 kJ·mol^{-1}). The results confirm that the reactant molecules were easier to be activated in the systems employing the -IN catalysts than that over the -IMP catalysts, suggesting that combination of the *in situ* encapsulation synthesis with zeolite nanosheets is a good strategy to prepare active and stable reforming catalysts for high temperature reactions.

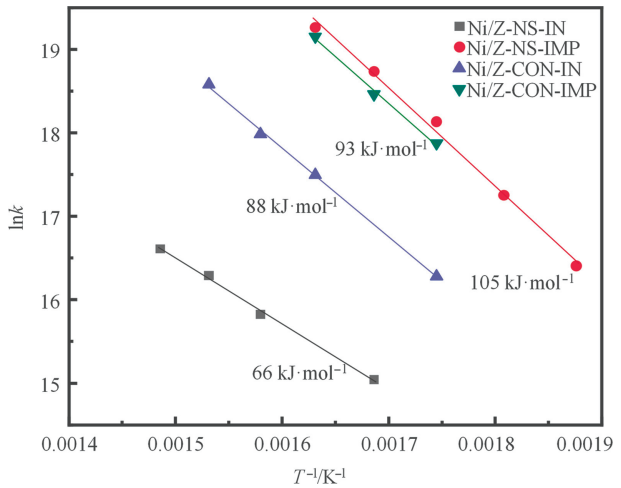

Fig. 8. Arrhenius plots to estimate E_a of the catalytic ESR over the four catalysts under investigation.

4. Conclusions

This study investigated the effects of the carrier morphology and catalyst preparation method on the performance of the resulting Ni catalysts in ESR for H_2 production. The results from comprehensive characterization showed that, compared to the conventional impregnation, the *in situ* encapsulation method is more appropriate to immobilize small Ni nanoparticles within the zeolite (ZSM-5) framework due to the confinement effect. It can constrain the size and shape of Ni nanoparticles within the carrier and inhibit aggregation and sintering during thermal treatments and ESR catalysis. In comparison with the conventional ZSM-5 zeolite (Z-CON, with the typical crystal size of 0.5–2.3 μm), 2-D ZSM-5 nanosheets (Z-NS) are more beneficial to prepare good reforming catalysts. The lamella structure of Z-NS (consisting of laminated thin sheets of 10–20 nm, with the crystal size of about 200 nm) could offer high mesopore volume and accessibility to the Ni sites within them with the reduced diffusion resistance and improved molecular transport. The catalysis results suggest that the catalysts prepared by the *in situ* encapsulation method could promote ethanol conversion better than that by impregnation due to the formation of small Ni nanoparticles which could reduce the activation barrier of ESR. Also, the catalysts based on Z-NS could improve H_2 yield compared to that based on Z-CON due to the improved local mass transfer to suppress side reactions in ESR. Accordingly, by combining the *in situ* encapsulation synthesis with Z-NS, we prepared the encapsulated Ni in Z-NS catalyst (*i.e.*, Ni/Z-NS-IN) which showed the comparative best performance in this study with a stable H_2 yield of ~65% (at 550 °C) for 48 h. The Ni/Z-NS-IN also showed good performance in mitigating sintering and coking during ESR, *e.g.*, ~16%(mass) coke disposition was measured by TGA for Ni/Z-NS-IN, whilst about 32%(mass) was found for the catalysts prepared by the conventional impregnation method. This work demonstrates that tuning of the catalyst synthesis method and carrier morphology could be a good strategy to prepare active and stable reforming catalysts for high temperature reactions.

Declaration of Interests

The authors declare that they have no known competing financial interests or personal relationships that could have appeared to influence the work reported in this paper.

Acknowledgements

This project has received funding from the European Union's Horizon 2020 Research and Innovation Program (872102). P.S. thanks the Science Achievement Scholarship of Thailand (SAST) for her research secondment at The University of Manchester. Y.J. thanks the National Natural Science Foundation of China (22378407) for funding.

Supplementary Material

Supplementary data to this article can be found online at https://doi.org/10.1016/j.cjche.2023.12.006.

References

[1] M. Balat, M. Balat, Political, economic and environmental impacts of biomass-based hydrogen, *Int. J. Hydrogen Energy* 34 (9) (2009) 3589–3603.

[2] H. Xiang, R.J. Xin, N. Prasongthum, P. Natewong, T. Sooknoi, J.W. Wang, P. Reubroycharoen, X.L. Fan, Catalytic conversion of bioethanol to value-added chemicals and fuels: A review, *Resour. Chem. Mater.* 1 (1) (2022) 47–68.

[3] B. Cifuentes, J. Gómez, N. Sánchez, L. Proaño, F. Bustamante, M. Cobo, Bio-ethanol steam reforming over monoliths washcoated with $RhPt/CeO_2–SiO_2$: The use of residual biomass to stably produce syngas, *Int. J. Hydrogen Energy* 46 (5) (2021) 4007–4018.

[4] N. Sanchez, R. Ruiz, V. Hacker, M. Cobo, Impact of bioethanol impurities on steam reforming for hydrogen production: A review, *Int. J. Hydrogen Energy* 45 (21) (2020) 11923–11942.

[5] O. Shtyka, Z. Dimitrova, R. Ciesielski, A. Kedziora, G. Mitukiewicz, J. Leyko, W. Maniukewicz, A. Czylkowska, T. Maniecki, Steam reforming of ethanol for hydrogen production: Influence of catalyst composition (Ni/Al_2O_3, $Ni/Al_2O_3–CeO_2$, $Ni/Al_2O_3–ZnO$) and process conditions, *React. Kinet. Mech. Catal.* 132 (2) (2021) 907–919.

[6] M. Kourtelesis, T.S. Moraes, L.V. Mattos, D.K. Niakolas, F.B. Noronha, X. Verykios, The effects of support morphology on the performance of Pt/CeO_2 catalysts for the low temperature steam reforming of ethanol, *Appl. Catal. B Environ.* 284 (2021) 119757.

[7] T.S. Moraes, L.E.P. Borges, R. Farrauto, F.B. Noronha, Steam reforming of ethanol on $Rh/SiCeO_2$ washcoated monolith catalyst: Stable catalyst performance, *Int. J. Hydrogen Energy* 43 (1) (2018) 115–126.

[8] S. Yoo, S. Park, J.H. Song, D.H. Kim, Hydrogen production by the steam reforming of ethanol over K-promoted $Co/Al_2O_3–CaO$ xerogel catalysts, *Mol. Catal.* 491 (2020) 110980.

[9] A. Di Michele, A. Dell'Angelo, A. Tripodi, E. Bahadori, F. Sànchez, D. Motta, N. Dimitratos, I. Rossetti, G. Ramis, Steam reforming of ethanol over $Ni/MgAl_2O_4$ catalysts, *Int. J. Hydrogen Energy* 44 (2) (2019) 952–964.

[10] T. Nejat, P. Jalalinezhad, F. Hormozi, Z. Bahrami, Hydrogen production from steam reforming of ethanol over Ni-Co bimetallic catalysts and MCM-41 as support, *J. Taiwan Inst. Chem. Eng.* 97 (2019) 216–226.

[11] I. Rossetti, M. Compagnoni, E. Finocchio, G. Ramis, A. Di Michele, A. Zucchini, S. Dzwigaj, Syngas production *via* steam reforming of bioethanol over Ni–BEA catalysts: A BTL strategy, *Int. J. Hydrogen Energy* 41 (38) (2016) 16878–16889.

[12] S.S. Xu, T.J.A. Slater, H. Huang, Y.T. Zhou, Y.L. Jiao, C.M.A. Parlett, S.L. Guan, S. Chansai, S.J. Xu, X.R. Wang, C. Hardacre, X.L. Fan, Developing silicalite-1 encapsulated Ni nanoparticles as sintering-/coking-resistant catalysts for dry reforming of methane, *Chem. Eng. J.* 446 (2022) 137439.

[13] P. Wetchasat, S. Salakhum, T. Imyen, D. Suttipat, W. Wannapakdee, M. Ketkaew, A. Prasertsab, P. Kidkhunthod, T. Witoon, C. Wattanakit, One-pot synthesis of ultra-small Pt dispersed on hierarchical zeolite nanosheet surfaces for mild hydrodeoxygenation of 4-propylphenol, *Catalysts* 11 (3) (2021) 333.

[14] R. Kore, R. Srivastava, B. Satpati, ZSM-5 zeolite nanosheets with improved catalytic activity synthesized using a new class of structure-directing agents, *Chemistry* 20 (36) (2014) 11511–11521.

[15] Y. Gao, B.H. Zheng, G. Wu, F.W. Ma, C.T. Liu, Effect of the Si/Al ratio on the performance of hierarchical ZSM-5 zeolites for methanol aromatization, *RSC Adv.* 6 (87) (2016) 83581–83588.

[16] Q.M. Sun, N. Wang, Q.M. Bing, R. Si, J.Y. Liu, R.S. Bai, P. Zhang, M.J. Jia, J.H. Yu, Subnanometric hybrid $Pd\text{-}M(OH)_2$, M = Ni, Co, clusters in zeolites as highly efficient nanocatalysts for hydrogen generation, *Chem* 3 (3) (2017) 477–493.

[17] M. Pérez-Page, J. Makel, K. Guan, S.L. Zhang, J. Tringe, R.H.R. Castro, P. Stroeve, Gas adsorption properties of ZSM-5 zeolites heated to extreme temperatures, *Ceram. Int.* 42 (14) (2016) 15423–15431.

[18] M.C. Tang, L. Xu, M.H. Fan, Effect of Ce on 5 wt% Ni/ZSM-5 catalysts in the CO_2 reforming of CH_4 reaction, *Int. J. Hydrogen Energy* 39 (28) (2014) 15482–15496.

[19] J. Grand, H. Awala, S. Mintova, Mechanism of zeolites crystal growth: New findings and open questions, *CrystEngComm* 18 (5) (2016) 650–664.

[20] F.X. Feng, L. Wang, X.W. Zhang, Q.F. Wang, Self-pillared ZSM-5-supported Ni nanoparticles as an efficient catalyst for upgrading oleic acid to aviation-fuel-range-alkanes, *Ind. Eng. Chem. Res.* 58 (29) (2019) 13112–13121.

[21] Z.P. Hu, C.C. Weng, C. Chen, Z.Y. Yuan, Catalytic decomposition of ammonia to CO_x-free hydrogen over Ni/ZSM-5 catalysts: A comparative study of the preparation methods, *Appl. Catal. Gen.* 562 (2018) 49–57.

[22] Y. Cui, J. Qiu, B. Chen, L.L. Xu, M.D. Chen, C.E. Wu, G. Cheng, B. Yang, N. Wang, X. Hu, CO_2 methanation over Ni/ZSM-5 catalysts: The effects of support morphology and La_2O_3 modification, *Fuel* 324 (2022) 124679.

[23] B. Sarkar, R. Tiwari, R.K. Singha, S. Suman, S. Ghosh, S.S. Acharyya, K. Mantri, L. N.S. Konathala, C. Pendem, R. Bal, Reforming of methane with CO_2 over Ni nanoparticle supported on mesoporous ZSM-5, *Catal. Today* 198 (1) (2012) 209–214.

[24] B. Saini, A.P. Tathod, J. Diwakar, S. Arumugam, N. Viswanadham, Nickel nanoparticles confined in ZSM-5 framework as an efficient catalyst for selective hydrodeoxygenation of lignin-derived monomers, *Biomass Bioenergy* 157 (2022) 106350.

[25] Y.L. Jiao, L. Forster, S.J. Xu, H.H. Chen, J.F. Han, X.Q. Liu, Y.T. Zhou, J.M. Liu, J.S. Zhang, J.H. Yu, C. D'Agostino, X.L. Fan, Creation of Al-enriched mesoporous ZSM-5 nanoboxes with high catalytic activity: Converting tetrahedral extra-framework Al into framework sites by post treatment, *Angew. Chem. Int. Ed Engl.* 59 (44) (2020) 19478–19486.

[26] D. Hartanto, L. Sin Yuan, S. Mutia Sari, D. Sugiarso, I. Kris Murwarni, T. Ersam, D. Prasetyoko, H. Nur, The use of the combination of ftir, pyridine adsorption, ^{27}Al and ^{29}Si MAS NMR to determine the brönsted and lewis acidic sites, *J. Teknologi* 78 (6) (2016) 223–228.

[27] S. Inagaki, N. Yamada, M. Nishii, Y. Nishi, Y. Kubota, Control of framework Al distribution in ZSM-5 zeolite *via* post-synthetic $TiCl_4$ treatment, *Microporous Mesoporous Mater.* 302 (2020) 110223.

[28] F. Frusteri, G. Bonura, Compendium of Hydrogen Energy, Woodhead Publishing, Oxford, 2015.

[29] M.D. Zhurka, A.A. Lemonidou, J.A. Anderson, P.N. Kechagiopoulos, Kinetic analysis of the steam reforming of ethanol over Ni/SiO_2 for the elucidation of metal-dominated reaction pathways, *React. Chem. Eng.* 3 (6) (2018) 883–897.

[30] F.X. Feng, X.P. Niu, L. Wang, X.W. Zhang, Q.F. Wang, TEOS-modified Ni/ZSM-5 nanosheet catalysts for hydroconversion of oleic acid to high-performance aviation fuel: Effect of acid spatial distribution, *Microporous Mesoporous Mater.* 291 (2020) 109705.

[31] M. Benito, J.L. Sanz, R. Isabel, R. Padilla, R. Arjona, L. Daza, Bio-ethanol steam reforming: Insights on the mechanism for hydrogen production, *J. Power Sources* 151 (2005) 11–17.

[32] A.N. Fatsikostas, X.E. Verykios, Reaction network of steam reforming of ethanol over Ni-based catalysts, *J. Catal.* 225 (2) (2004) 439–452.

[33] B. Roy, U. Martinez, K. Loganathan, A.K. Datye, C.A. Leclerc, Effect of preparation methods on the performance of Ni/Al_2O_3 catalysts for aqueous-phase reforming of ethanol: Part I-catalytic activity, *Int. J. Hydrogen Energy* 37 (10) (2012) 8143–8153.

[34] D.J. Haynes, D. Shekhawat, Fuel Cells: Technologies for Fuel Processing, Elsevier, Amsterdam, 2011.

[35] M. Pudukudy, Z. Yaakob, Methane decomposition over Ni, Co and Fe based monometallic catalysts supported on sol gel derived SiO_2 microflakes, *Chem. Eng. J.* 262 (2015) 1009–1021.

[36] B.D. Gould, X.Y. Chen, J.W. Schwank, *n*-Dodecane reforming over nickel-based monolith catalysts: Deactivation and carbon deposition, *Appl. Catal. Gen.* 334 (1–2) (2008) 277–290.

[37] A.G. Bannov, M.V. Popov, P.B. Kurmashov, Thermal analysis of carbon nanomaterials: Advantages and problems of interpretation, *J. Therm. Anal. Calorim.* 142 (1) (2020) 349–370.

[38] A.A.S. Gonçalves, P.B. Faustino, J.M. Assaf, M. Jaroniec, One-pot synthesis of mesoporous Ni-Ti-Al ternary oxides: Highly active and selective catalysts for steam reforming of ethanol, *ACS Appl. Mater. Interfaces* 9 (7) (2017) 6079–6092.

[39] S.Y. Wang, B. He, R. Tian, X. Wu, X. An, Y.P. Liu, J. Su, Z.H. Yu, X.M. Xie, Novel core-shell-like Ni-supported hierarchical beta zeolite catalysts on bioethanol steam reforming, *Int. J. Hydrogen Energy* 45 (33) (2020) 16409–16420.

[40] A. Kumar, R. Prasad, Y.C. Sharma, Ethanol steam reforming study over ZSM-5 supported cobalt *versus* nickel catalyst for renewable hydrogen generation, *Chin. J. Chem. Eng.* 27 (3) (2019) 677–684.

[41] A. Rodriguez-Gomez, A. Caballero, Bimetallic Ni-Co/SBA-15 catalysts for reforming of ethanol: How cobalt modifies the nickel metal phase and product distribution, *Mol. Catal.* 449 (2018) 122–130.

[42] J. Vicente, C. Montero, J. Ereña, M.J. Azkoiti, J. Bilbao, A.G. Gayubo, Coke deactivation of Ni and Co catalysts in ethanol steam reforming at mild temperatures in a fluidized bed reactor, *Int. J. Hydrogen Energy* 39 (24) (2014) 12586–12596.